

Performance Analysis of a 2D-MUSIC Algorithm for Parametric Near-Field Channel Estimation

Doğa Gürçünoğlu*, Alva Kosasih*, Parisa Ramezani*, Özlem Tuğfe Demir[†], Emil Björnson*, Gábor Fodor*[†]

*School of EECS, KTH Royal Institute of Technology, Stockholm, Sweden ({dogag,kosasih,parram,emilbjo,gaborf}@kth.se)

[†]Ericsson Research AB, Stockholm, Sweden ({doga.gurgunoglu,gabor.fodor}@ericsson.com)

[‡]Department of Electrical-Electronics Engineering, TOBB ETU, Ankara, Turkey (ozlemtugfedemir@etu.edu.tr)

Abstract—In this letter, we address parametric channel estimation in a multi-user multiple-input multiple-output system within the radiative near-field of the base station array with aperture antennas. We investigate a two-dimensional multiple signal classification algorithm (2D-MUSIC) to estimate both the range and the azimuth angles of arrival for the users' channels, utilizing parametric radiative near-field channel models. We analyze the performance of the algorithm by deriving the Cramér-Rao bound (CRB) for parametric estimation, and its effectiveness is compared against the least squares estimator, which is a non-parametric estimator. Numerical results indicate that the 2D-MUSIC algorithm outperforms the least squares estimator. Furthermore, the results demonstrate that the performance of 2D-MUSIC achieves the parametric channel estimation CRB, which shows that the algorithm is asymptotically consistent.

Index Terms—Radiative near-field, aperture antennas, MUSIC, channel estimation, Cramér-Rao lower bound.

I. INTRODUCTION

The success of massive multiple-input multiple-output (M-MIMO) implementation in 5G systems, across both sub-6 GHz and mmWave bands, suggests that the next generation of wireless systems will likely exploit even larger arrays, referred to as the extremely large aperture array (ELAA) [1]–[3]. Moreover, there is an ongoing trend toward employing higher frequencies, implying a smaller wavelength in wireless systems [4], [5]. As the array size increases and the wavelength shrinks, the Fraunhofer array distance, the boundary between radiative near- and far-fields, becomes large. Consequently, a user equipment (UE) is likely to fall into the radiative near-field region of the ELAA [6], [7]. In the radiative near-field, the spherical curvature of the wavefront is noticeable; therefore, there are spherical phase variations between the antenna elements in the ELAA. The phase variations must be characterized by both the angle and distance between the ELAA and the transmitter. This renders far-field channel models inaccurate as the far-field array response does not capture information about the propagation distance.

To address this issue, polar-domain representation for the extremely large-scale MIMO (XL-MIMO) channel has been proposed in [8], [9]. Reference [8] focuses on the recovery of the angular and distance information in the near-field

channel utilizing the sparsity in the polar domain, while [9] utilizes the distance domain in addition to the angular domain to multiplex UEs in line-of-sight (LOS) scenarios. With the polar-domain representation, one can sample both the angular and the distance domains to obtain a near-field codebook. Moreover, the polar-domain representation is used to ensure a sparse representation of the near-field channel, enabling the utilization of compressive sensing methods and classical algorithms [8].

As recent papers [10]–[13] indicate, in short-range MIMO communication scenarios, the LOS propagation channel is dominating, and LoS models serve as a good approximation of the real propagation conditions for deriving bounds for channel estimation algorithms. When the channel is pure-LOS, another way to estimate the near-field channel is to first estimate the parameters of the UEs' locations, given that the channel has a simple and known parametrization. Subsequently, the parameters are substituted into the channel parametric model to yield the channel estimate. The state-of-the-art [7] focuses on developing a low-complexity algorithm to estimate the parameters of the UE' locations by performing subsequential parameter estimations neglecting the correlation between the parameters. However, this introduces notable performance degradation. Furthermore, no theoretical bound is derived to benchmark the performance of the estimator.

In this letter, we explore the possibility of estimating the UEs' locations in polar coordinates based on the 2D near-field channel model, where the channel is assumed to be pure-LOS, as in [10], [11]. Then, we use the parameter estimates to infer the channel coefficients. More importantly, we derive the Cramér-Rao bound (CRB) on the parametric channel estimation mean squared error (MSE) to evaluate the performance of the 2D-multiple signal classification (MUSIC) estimator. The CRB provides a lower bound on the variance of any unbiased estimator [14], and depends heavily on the relationship between the observation and the parameter. Therefore, it is useful in evaluating parametric estimators. In [15], the CRB on parametric channel estimation is derived with a far-field model for a system using two reconfigurable intelligent surfaces by considering the non-parametric CRB as a transitional step towards a parametric channel estimation CRB. To the best of the authors' knowledge, however, such an analysis has not been used to evaluate the performance

This study is supported by EU Horizon 2020 MSCA-ITN-METAWIRELESS, Grant Agreement 956256. This paper was supported by the Grant 2019-05068 from the Swedish Research Council. G. Fodor was supported by the 6G-MUSICAL EU project, ID: 101139176.

of parametric channel estimators. In this letter, we explore the opportunities of parametric channel estimation in near-field channels with aperture antennas by performing the aforementioned analysis. In addition to the CRB analysis, we also compare the performance of the 2D-MUSIC algorithm with a non-parametric estimator, namely, the least squares (LS) estimator to observe the performance gain from parametric channel estimation.

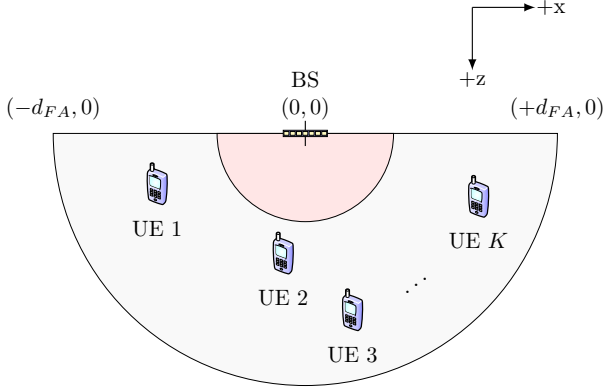


Fig. 1: An illustration of the system setup (not to scale). The radius of the region highlighted with red color is twice the aperture length of the antenna, within which we assume that no UEs are present, and we assume that all K users are within the radiative near field of the array.

II. SYSTEM MODEL

We consider a base station (BS) equipped with a uniform linear array (ULA) consisting of N aperture antennas, serving K single-antenna UEs.¹ The location of UE k is denoted as $(x_k, 0, z_k)$, which is assumed to be in the radiative near-field region (Fresnel region) of the BS array, for $k \in \{1, \dots, K\}$. Without loss of generality, we let the BS be geometrically arranged along the x -axis with half-wavelength spacing, and the array is centered around $(0, 0, 0)$. A geometric illustration of the system setup is provided in Fig. 1.

Antenna element n is centered at $(\bar{x}_n, 0, 0)$ with

$$\bar{x}_n = \underbrace{\left(n - \frac{N+1}{2}\right)}_{\delta_n} \underbrace{\frac{\lambda}{2}}_{\Delta}, \quad (1)$$

where δ_n and Δ are the index of antenna element n , for $n = 1, \dots, N$, and spacing between two antenna elements, respectively. The aperture antennas each have an area of Δ^2 along the xy -plane.

The channel between antenna element n and UE k located at the distance d_k (from the origin) in the azimuth angle φ_k with respect to the origin (measured from x -axis towards the z -axis) is represented as

$$h_n^k(d_k, \varphi_k) = \sqrt{\beta_{n,k}} e^{-j\frac{2\pi}{\lambda} r_n^k}, \quad (2)$$

where $r_n^k = \sqrt{d_k^2 + (\delta_n \Delta)^2 - 2d_k \Delta \delta_n \cos(\varphi_k)}$. The free-space channel gain $\beta_{n,k}$ between antenna n (which has size

$\lambda/2 \times \lambda/2$) and UE k can be approximated as [6, Eqn. (69)], [16]

$$\begin{aligned} \beta_{n,k} &= \int_{\bar{x}_n - \lambda/4}^{\bar{x}_n + \lambda/4} \int_{-\lambda/4}^{\lambda/4} \frac{1}{4\pi} \frac{z_k((x-x_k)^2 + z_k^2)}{((x-x_k)^2 + y^2 + z_k^2)^{5/2}} dx dy \\ &\approx \frac{\lambda^2}{4} \frac{1}{4\pi} \frac{z_k((\bar{x}_n - x_k)^2 + z_k^2)}{((\bar{x}_n - x_k)^2 + 0^2 + z_k^2)^{5/2}} \\ &\approx \frac{\lambda^2}{16\pi} \frac{d_k \sin(\varphi_k)}{d_k^3} = \frac{\lambda^2}{16\pi} \frac{\sin(\varphi_k)}{d_k^2} = \beta_k \end{aligned} \quad (3)$$

which gives a sine-shaped antenna pattern with a maximum gain of π . The approximation holds when the propagation distance is larger than twice the array aperture [6] so that the spherical amplitude variations over the wavefront are negligible but not the phase variations. Using (2) and (3), we can model the near-field channel vector to UE k as

$$\mathbf{h}_k(d_k, \varphi_k) = \sqrt{\beta_k} \left[e^{-j\frac{2\pi}{\lambda} r_1^k} \dots e^{-j\frac{2\pi}{\lambda} r_N^k} \right]^T. \quad (4)$$

At time instance l , the received signal can be written as

$$\mathbf{y}[l] = \mathbf{H}\mathbf{s}[l] + \mathbf{w}[l], \quad l = 1, \dots, L, \quad (5)$$

where $\mathbf{H} = [\mathbf{h}_1(d_1, \varphi_1) \dots \mathbf{h}_K(d_K, \varphi_K)]$, $\mathbf{y}[l] = [y_1[l] \dots y_N[l]]^T$ contains the received signals, $\mathbf{s}[l] = [s_1[l] \dots s_K[l]]^T$ represents the transmitted signals from K UEs, and $\mathbf{w}[l] = [w_1[l] \dots w_N[l]]^T$ is the additive noise where each entry follows an independent complex Gaussian distribution with zero mean and variance σ^2 .

III. NEAR-FIELD PARAMETRIC CHANNEL ESTIMATION VIA 2D-MUSIC

In this section, our aim is to estimate the channels $\mathbf{h}_k(d_k, \varphi_k)$ for $k = 1, \dots, K$ based on (5). Combining L such observations over time, we first aim to estimate the ranges d_k and azimuth angle of arrivals (AoAs) φ_k for $k = 1, \dots, K$ using the 2D-MUSIC algorithm. The channel response function, defined in (2), allows us to characterize the UEs' channels by estimating the locations (d_k, φ_k) , $k = 1, \dots, K$, from L transmissions at distinct instants. This allows us to estimate the channels of the K UEs based on the d_k and φ_k by using the parametric model in (4). In the following, we provide a way to utilize 2D-MUSIC to estimate the UEs' channels. We assume that: 1) The UEs are not located in exactly the same angular directions. 2) The transmitted signals are assumed to follow a circular symmetric complex Gaussian distribution. 3) The noise is independent of all the signals.

The MUSIC algorithm works by exploiting the structure of the eigenvectors in the sample covariance matrix [17]:

$$\hat{\mathbf{R}}_L = \frac{1}{L} \sum_{l=1}^L \mathbf{y}[l] \mathbf{y}^H[l]. \quad (6)$$

Given the number of UEs K , we first construct the noise-subspace matrix $\hat{\mathbf{U}}_n \in \mathbb{C}^{N \times (N-K)}$ whose columns are the eigenvectors of $\hat{\mathbf{R}}_L$ corresponding to the smallest $(N-K)$ eigenvalues. Then, the 2D MUSIC spectrum is generated as

$$S(d, \varphi) = \frac{1}{\mathbf{h}^H(d, \varphi) \hat{\mathbf{U}}_n \hat{\mathbf{U}}_n^H \mathbf{h}(d, \varphi)}, \quad (7)$$

¹Note that the model is extendable to a uniform planar array (UPA), as it was shown in [7].

where each possible value of $\mathbf{h}(d, \varphi)$ is obtained by computing the potential channel responses by plugging the grid points into (4). K combinations of (d, φ) corresponding to the peaks in the MUSIC spectrum are then identified, each representing a UE's location. The channel estimate $\hat{\mathbf{H}}$ can then be obtained by substituting the parameter estimates $(d_k, \varphi_k), k = 1, \dots, K$ into (2).

IV. CRB ON NEAR-FIELD PARAMETRIC CHANNEL ESTIMATION

In parameter estimation problems, bounds on estimation performance serve as the golden standard to evaluate the performance of estimators. To this end, we derive the CRB on the near-field parametric channel estimation in this section. The CRB, the inverse of the Fisher Information Matrix (FIM), provides a lower bound on the performance of any unbiased estimator [14] via the following matrix inequality:

$$\text{Cov}(\hat{\boldsymbol{\theta}}(\mathbf{X})) \succeq \mathbf{I}^{-1}(\mathbf{X}; \boldsymbol{\theta}) \quad (8)$$

for an estimate of a parameter vector $\boldsymbol{\theta}$ based on an observation vector \mathbf{X} . Here, $\text{Cov}(\hat{\boldsymbol{\theta}}(\mathbf{X})) = \mathbb{E}[(\hat{\boldsymbol{\theta}}(\mathbf{X}) - \boldsymbol{\theta})(\hat{\boldsymbol{\theta}}(\mathbf{X}) - \boldsymbol{\theta})^H]$ is the covariance matrix and, consequently, the bound on the sum MSE can be expressed as

$$\mathbb{E} \left[\left\| \hat{\boldsymbol{\theta}}(\mathbf{X}) - \boldsymbol{\theta} \right\|^2 \right] \geq \text{tr}(\mathbf{I}^{-1}(\mathbf{X}; \boldsymbol{\theta})). \quad (9)$$

In a generic vector parameter estimation problem, the FIM is computed via the following equation [18, Eq. 3.21]:

$$[\mathbf{I}(\mathbf{X}; \boldsymbol{\theta})]_{i,j} = -\mathbb{E} \left[\frac{\partial^2 \ln(f(\mathbf{X}; \boldsymbol{\theta}))}{\partial \theta_i \partial \theta_j} \right], \quad (10)$$

where θ_i is the i -th element of $\boldsymbol{\theta}$. In our near-field parametric channel estimation problem, the observation from a single transmission is stated in (5). Before ensembling the observations from multiple transmissions, it is more convenient to change the order of the transmitted signals and the unknown channel in (5) as

$$\mathbf{y}[l] = \underbrace{\begin{bmatrix} s_1[l] \mathbf{I}_N & \dots & s_K[l] \mathbf{I}_N \end{bmatrix}}_{\triangleq \mathbf{S}[l] \in \mathbb{C}^{N \times NK}} \underbrace{\begin{bmatrix} \mathbf{h}_1(d_1, \varphi_1) \\ \vdots \\ \mathbf{h}_K(d_K, \varphi_K) \end{bmatrix}}_{\triangleq \tilde{\mathbf{h}}(\boldsymbol{\theta}) \in \mathbb{C}^{NK \times 1}} + \mathbf{w}[l], \quad (11)$$

where $\boldsymbol{\theta} \triangleq [d_1 \dots d_K \varphi_1 \dots \varphi_K]^T \in \mathbb{R}^{2K}$. While (11) corresponds to the observation from a single transmission, we can stack the observations from multiple transmissions $l = 1, \dots, L$ vertically to obtain

$$\tilde{\mathbf{y}} = \tilde{\mathbf{S}} \tilde{\mathbf{h}}(\boldsymbol{\theta}) + \tilde{\mathbf{w}} \in \mathbb{C}^{LN \times 1}, \quad (12)$$

where $\tilde{\mathbf{y}} \triangleq [\mathbf{y}^T[1] \dots \mathbf{y}^T[L]]^T \in \mathbb{C}^{LN}$, $\tilde{\mathbf{S}} \triangleq [\mathbf{S}^T[1] \dots \mathbf{S}^T[L]]^T \in \mathbb{C}^{LN \times NK}$, and $\tilde{\mathbf{w}} \triangleq [\mathbf{w}^T[1] \dots \mathbf{w}^T[L]]^T \in \mathbb{C}^{LN}$. To compute the FIM, we first define a transition parameter $\mathbf{v} \triangleq \tilde{\mathbf{h}}(\boldsymbol{\theta})$, for which we can express the FIM as

$$\mathbf{I}(\tilde{\mathbf{y}}; \mathbf{v}) = \mathbf{S}^H \boldsymbol{\Sigma}_{\tilde{\mathbf{w}}}^{-1} \mathbf{S}, \quad (13)$$

where $\boldsymbol{\Sigma}_{\tilde{\mathbf{w}}} = \mathbb{E}[\tilde{\mathbf{w}} \tilde{\mathbf{w}}^H] \in \mathbb{C}^{LN \times LN}$ is the noise covariance matrix, which has the following relationship with the noise covariance for a single transmission $\boldsymbol{\Sigma}_{\mathbf{w}} = \mathbb{E}[\mathbf{w} \mathbf{w}^H] \in \mathbb{C}^{N \times N}$:

$$\boldsymbol{\Sigma}_{\tilde{\mathbf{w}}} = \mathbf{I}_L \otimes \boldsymbol{\Sigma}_{\mathbf{w}} = \sigma^2 \mathbf{I}_{LN}. \quad (14)$$

This relation holds since the noise is independent over both time and antennas.

A. CRB for Vector Transformations

To incorporate the parametric nature of the channel into the CRB analysis, we consider the parametric model $\tilde{\mathbf{h}}(\cdot) : \mathbb{R}^{2K} \mapsto \mathbb{C}^{NK}$ as a vector transformation to utilize the following identity [18, Eq. 3.30]:

$$\mathbf{I}^{-1}(\tilde{\mathbf{y}}; \mathbf{v}) = \mathbf{J}_{\tilde{\mathbf{h}}}^H \mathbf{I}^{-1}(\tilde{\mathbf{y}}; \boldsymbol{\theta}) \mathbf{J}_{\tilde{\mathbf{h}}}, \quad (15)$$

where $\mathbf{J}_{\tilde{\mathbf{h}}} \in \mathbb{C}^{2K \times NK}$ is the Jacobian of the non-linear transformation $\tilde{\mathbf{h}} : \mathbb{R}^{2K} \mapsto \mathbb{C}^{NK}$ with entries $[\mathbf{J}_{\tilde{\mathbf{h}}}]_{i,j} = \frac{\partial \tilde{\mathbf{h}}_i}{\partial \theta_j}$. While (15) suffices to obtain the inverse FIM between the observation and the location parameters, the non-parametric FIM in (13) is not always invertible. Therefore, it is more desirable to have an expression for $\mathbf{I}(\tilde{\mathbf{y}}; \boldsymbol{\theta})$ in terms of $\mathbf{I}(\tilde{\mathbf{y}}; \mathbf{v})$. To this end, we multiply (15) with the pseudoinverse of $\mathbf{J}_{\tilde{\mathbf{h}}}$ from both sides to obtain

$$\mathbf{I}^{-1}(\tilde{\mathbf{y}}; \boldsymbol{\theta}) = (\mathbf{J}_{\tilde{\mathbf{h}}} \mathbf{J}_{\tilde{\mathbf{h}}}^H)^{-1} \mathbf{J}_{\tilde{\mathbf{h}}} \mathbf{I}^{-1}(\tilde{\mathbf{y}}; \mathbf{v}) \mathbf{J}_{\tilde{\mathbf{h}}}^H (\mathbf{J}_{\tilde{\mathbf{h}}} \mathbf{J}_{\tilde{\mathbf{h}}}^H)^{-1}, \quad (16)$$

which is the $2K \times 2K$ inverse FIM between the received signals and the UEs' coordinates. Applying (15) again to get the parametric channel estimation CRB, we obtain

$$\begin{aligned} \mathbf{I}^{-1}(\tilde{\mathbf{y}}; \tilde{\mathbf{h}}(\boldsymbol{\theta})) &= \mathbf{J}_{\tilde{\mathbf{h}}}^H \mathbf{I}^{-1}(\tilde{\mathbf{y}}; \boldsymbol{\theta}) \mathbf{J}_{\tilde{\mathbf{h}}}, \\ &= \mathbf{J}_{\tilde{\mathbf{h}}}^H (\mathbf{J}_{\tilde{\mathbf{h}}} \mathbf{J}_{\tilde{\mathbf{h}}}^H)^{-1} \mathbf{J}_{\tilde{\mathbf{h}}} \mathbf{I}^{-1}(\tilde{\mathbf{y}}; \mathbf{v}) \mathbf{J}_{\tilde{\mathbf{h}}}^H (\mathbf{J}_{\tilde{\mathbf{h}}} \mathbf{J}_{\tilde{\mathbf{h}}}^H)^{-1} \mathbf{J}_{\tilde{\mathbf{h}}}. \end{aligned} \quad (17)$$

Note that both $\mathbf{I}^{-1}(\tilde{\mathbf{y}}; \mathbf{v})$ and $\mathbf{I}^{-1}(\tilde{\mathbf{y}}; \tilde{\mathbf{h}}(\boldsymbol{\theta}))$ denote the inverse FIM for channel estimation. However, the latter contains additional information from the channel structure. Also note that $\mathbf{J}_{\tilde{\mathbf{h}}}^H (\mathbf{J}_{\tilde{\mathbf{h}}} \mathbf{J}_{\tilde{\mathbf{h}}}^H)^{-1} \mathbf{J}_{\tilde{\mathbf{h}}} \neq \mathbf{I}_{NK}$, hence these two matrices are different.

B. Jacobian of the Parametric Channel

To obtain the CRB on the MSE of any parametric estimator for our setup, what remains is to derive the Jacobian of $\tilde{\mathbf{h}}(\cdot)$ in closed form². Based on the definition of $\tilde{\mathbf{h}}$ in (11), the Jacobian can be obtained as $\mathbf{J}_{\tilde{\mathbf{h}}} = [\mathbf{J}_1^T, \mathbf{J}_2^T]^T$ where $\mathbf{J}_1, \mathbf{J}_2 \in \mathbb{C}^{K \times NK}$ are block diagonal matrices containing the partial derivatives of the channel with respect to d_k and φ_k , respectively. That is, $\mathbf{J}_1 = \text{diag} \left(\frac{\partial \mathbf{h}_1^T}{\partial d_1}, \dots, \frac{\partial \mathbf{h}_K^T}{\partial d_K} \right)$ and $\mathbf{J}_2 = \text{diag} \left(\frac{\partial \mathbf{h}_1^T}{\partial \varphi_1}, \dots, \frac{\partial \mathbf{h}_K^T}{\partial \varphi_K} \right)$. To derive $\frac{\partial \mathbf{h}_k}{\partial d_k}$ and $\frac{\partial \mathbf{h}_k}{\partial \varphi_k}$, we need to recall the near-field

²Note that by considering the parametric channel model for UPA in [7], we can obtain the CRB for the 3D case as well.

channel model parametrized by UE location in Section II. Starting from (4), we have

$$\begin{aligned} \frac{\partial \mathbf{h}_k}{\partial d_k} &= \frac{1}{2\sqrt{\beta_k}} \frac{\partial \beta_k}{\partial d_k} \left[e^{-j\frac{2\pi}{\lambda} r_1^k} \quad \dots \quad e^{-j\frac{2\pi}{\lambda} r_N^k} \right]^T \\ &+ \sqrt{\beta_k} \left[-j\frac{2\pi}{\lambda} \frac{\partial r_1^k}{\partial d_k} e^{-j\frac{2\pi}{\lambda} r_1^k} \quad \dots \quad -j\frac{2\pi}{\lambda} \frac{\partial r_N^k}{\partial d_k} e^{-j\frac{2\pi}{\lambda} r_N^k} \right]^T, \end{aligned} \quad (18a)$$

$$\begin{aligned} \frac{\partial \mathbf{h}_k}{\partial \varphi_k} &= \frac{1}{2\sqrt{\beta_k}} \frac{\partial \beta_k}{\partial \varphi_k} \left[e^{-j\frac{2\pi}{\lambda} r_1^k} \quad \dots \quad e^{-j\frac{2\pi}{\lambda} r_N^k} \right]^T \\ &+ \sqrt{\beta_k} \left[-j\frac{2\pi}{\lambda} \frac{\partial r_1^k}{\partial \varphi_k} e^{-j\frac{2\pi}{\lambda} r_1^k} \quad \dots \quad -j\frac{2\pi}{\lambda} \frac{\partial r_N^k}{\partial \varphi_k} e^{-j\frac{2\pi}{\lambda} r_N^k} \right]^T, \end{aligned} \quad (18b)$$

where $\frac{\partial \beta_k}{\partial d_k}$, $\frac{\partial \beta_k}{\partial \varphi_k}$, $\frac{\partial r_n^k}{\partial d_k}$, and $\frac{\partial r_n^k}{\partial \varphi_k}$ can be expressed as

$$\frac{\partial \beta_k}{\partial d_k} = -\frac{\lambda^2 \sin(\varphi_k)}{8\pi d_k^3}, \quad (19a)$$

$$\frac{\partial \beta_k}{\partial \varphi_k} = \frac{\lambda^2 \cos(\varphi_k)}{16\pi d_k^2}, \quad (19b)$$

$$\frac{\partial r_n^k}{\partial d_k} = \frac{d_k - \Delta \delta_n \cos(\varphi_k)}{\sqrt{d_k^2 + (\delta_n \Delta)^2 - 2d_k \Delta \delta_n \cos(\varphi_k)}}, \quad (19c)$$

$$\frac{\partial r_n^k}{\partial \varphi_k} = \frac{d_k \Delta \delta_n \sin(\varphi_k)}{\sqrt{d_k^2 + (\delta_n \Delta)^2 - 2d_k \Delta \delta_n \cos(\varphi_k)}}. \quad (19d)$$

As a result, we have $\mathbf{J}_{\tilde{\mathbf{h}}}$ and hence the CRB for parametric channel estimation in closed form.

V. NUMERICAL RESULTS

In this section, we provide numerical examples to demonstrate the performance of the 2D-MUSIC algorithm. As the state-of-the-art, we include a revised version of the proposed algorithm in [7]. While it was proposed as a 2D-1D-MUSIC algorithm, we implemented it as a 1D-1D-MUSIC algorithm in our case due to the fewer number of dimensions. Our version of this algorithm first estimates the azimuth angles and then estimates the ranges based on the azimuth angle estimates. In addition, we include a non-parametric channel estimator, namely, the LS estimator. Note that one disadvantage of the LS estimator is that it requires a known sequence of pilots while the 2D-MUSIC method does not. For all estimators, we use the CRB as the benchmark. Specifically, for the LS estimator, we use the non-parametric CRB (inverse of (13)) and for the 2D-MUSIC and the 1D-1D MUSIC estimator, we use the parametric CRB we derived in Section IV. In addition, we examine the impact of the location of the UE on the channel estimation performance by considering a two-UE setup, assigning one of the UEs a fixed location, and changing the location of the other UE. We provide the parameters used to generate the numerical results in Table I.

TABLE I: List of parameters used to generate the numerical results.

Parameter	Value
N	32
L	40
K	4 in Fig. 2, 2 in Fig. 3
SNR	-10, 0, ..., 60 dB
λ	10 cm

A. Performance of the 2D-MUSIC Algorithm

We first compare the estimation performance for the 2D-MUSIC algorithm, the 1D-1D-MUSIC algorithm, and the LS estimator. As shown in Table I, we consider the transmit signal-to-noise ratio (SNR) (P_p/σ^2) to be within the range of -10 dB and 60 dB. The UEs are dropped by selecting uniformly spaced points over the angular domain between 60° and 120° , and between twice the aperture size and the Fraunhofer array distance to ensure radiating near-field conditions. In Fig. 2, we provide the CRBs on the channel estimation normalized mean squared error (NMSE) for parametric and non-parametric estimators in blue and black solid lines, respectively³. Then, we provide the NMSEs achieved by the 2D-MUSIC algorithm, the 1D-1D-MUSIC, and the LS estimator with green, magenta, and red lines, respectively.

The parameter undergoes a known linear transformation when considering the system model non-parametrically. Then, it is corrupted by additive Gaussian noise with known statistics. Therefore, the LS estimator achieves the CRB exactly. On the other hand, the 2D-MUSIC algorithm performs worse than the parametric CRB at low SNR, where the algorithm performance is noise-limited. When the SNR is higher than 10 dB, however, the 2D-MUSIC algorithm performance achieves the parametric CRB, showing that the MUSIC algorithm is asymptotically consistent. While 2D-MUSIC would follow the CRB at higher SNR, it starts to show granularity-limited behavior after 30 dB SNR. In addition, note that 2D-MUSIC consistently outperforms LS until 50 dB SNRs, and is then outperformed by LS due to granularity limitation. In contrast, the 1D-1D MUSIC algorithm cannot achieve the CRB as the range estimation relies on the noisy angle estimates in the previous step. The NMSE of this estimator converges to a higher floor despite using the identical angle and range grids as 2D-MUSIC. Moreover, both 2D-MUSIC and LS estimators outperform 1D-1D MUSIC, which shows that it is not practical for our setup.

B. Location Dependence of the CRB

We will now demonstrate how the parametric CRB changes based on the UE location. To this end, we consider $K = 2$ UEs and fix the SNR to 40 dB. In addition, we fix the location of UE 1, denoted by the red dot in Fig. 3. Then, we compute the CRB on the parametric channel estimation NMSE for UE 2 over a rectangular region, as shown in Fig. 3, where the color bar shows the CRB value. While the antenna array is located at the origin, we choose our rectangular region so all the points are further than twice the aperture size and closer than the Fraunhofer distance to the antenna array.

Note that the CRB increases as the UE moves towards the sides of the region and as the distance increases. This is due to multiple factors. First, the channel gain decreases as the distance to the BS increases. However, the CRB trend would be radial if this were the sole factor. The additional factor

³Note that we apply the same normalization to the CRLB as to the MSE when obtaining the NMSE.

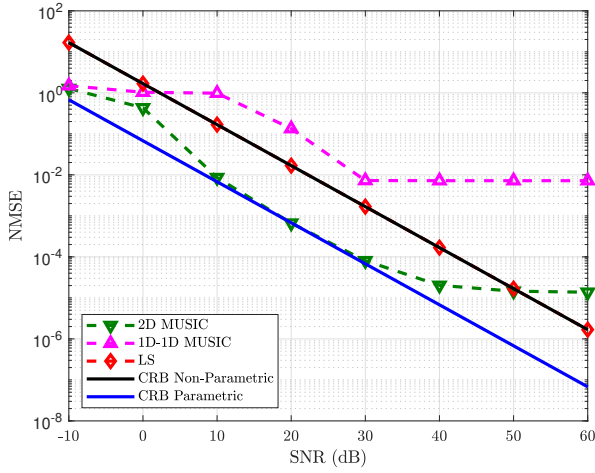


Fig. 2: SNR versus NMSEs of parametric and non-parametric channel estimation along with parametric and non-parametric CRBs, for the parameters specified in Table I. Note that the CRBs are computed based on the ensemble of observations over time and hence are valid for L pilot transmissions.

comes from parametric channel estimation as the non-linearity coming from the near field channel model causes the CRB to be a function of the true parameter value. In contrast, the performance is not affected by UE 2's proximity to UE 1. This is because there are enough observations and spatial degrees of freedom to accurately resolve the two UEs.

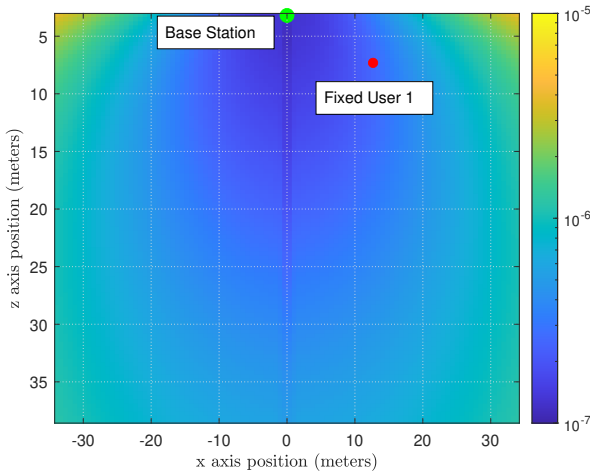


Fig. 3: CRB of channel estimation for the second UE when the first UE's location is fixed. The SNR is fixed at 40 dB. Note that the green dot shows the point closest to the BS which is located at (0, 0), and the plot starts from twice the aperture size distance, i.e. 3.2 m.

VI. CONCLUSIONS

In this letter, we considered the parametric channel estimation problem, where the UEs are within the radiative near field of the BS array. We used the 2D-MUSIC algorithm, which estimates the range and azimuth AoAs of the UEs' channels, and obtained the channel estimates using the parametric near-field channel models for aperture antennas. To evaluate the channel estimation performance of 2D-MUSIC, we derived the CRB of parametric channel estimation in closed form and

compared the 2D-MUSIC algorithm with a non-parametric estimator, namely the LS estimator. In addition, we considered the 2D adaptation of the state-of-the-art algorithm in [7], namely the 1D-1D-MUSIC. Our numerical results showed that 2D-MUSIC outperforms both the LS estimator and the 1D-1D-MUSIC algorithm, and achieves the parametric channel estimation CRB outside the noise-limited and granularity-limited regions. In addition, we also demonstrated that the 2D-MUSIC algorithm performance is close to the CRB and hence is an efficient method to estimate the channel parametrically.

REFERENCES

- [1] E. Björnson, L. Sanguinetti, H. Wymeersch, J. Hoydis, and T. L. Marzetta, "Massive MIMO is a reality—What is next? Five promising research directions for antenna arrays," *Digital Signal Processing*, vol. 94, pp. 3–20, Nov. 2019.
- [2] H. Wang, A. Kosasih, C. -K. Wen, S. Jin and W. Hardjawana, "Expectation propagation detector for extra-large scale massive MIMO," *IEEE Trans. Wireless Commun.*, vol. 19, no. 3, pp. 2036–2051, Mar. 2020.
- [3] A. Amiri, M. Angjelichinoski, E. de Carvalho, and R. W. Heath, "Extremely large aperture massive MIMO: Low complexity receiver architectures," in *Proc. IEEE Global Commun. Conf. Workshops*, UAE, Dec. 2018.
- [4] T. S. Rappaport et al., "Wireless communications and applications above 100 GHz: Opportunities and challenges for 6G and beyond," *IEEE Access*, vol. 7, pp. 78 729–78 757, June 2019.
- [5] L. Sanguinetti, E. Björnson, and J. Hoydis, "Toward massive MIMO 2.0: Understanding spatial correlation, interference suppression, and pilot contamination," *IEEE J. Sel. Areas Commun.*, vol. 68, no. 1, p. 232–257, Jan. 2020.
- [6] E. Björnson and L. Sanguinetti, "Power scaling laws and near-field behaviors of massive MIMO and intelligent reflecting surfaces," *IEEE Open J. of the Commun. Soc.*, vol. 1, pp. 1306–1324, Sept. 2020.
- [7] A. Kosasih, Ö. T. Demir, and E. Björnson, "Parametric near-field channel estimation for extremely large aperture arrays," in *2023 57th Asilomar Conference on Signals, Systems, and Computers*, 2023, pp. 162–166.
- [8] M. Cui and L. Dai, "Channel estimation for extremely large-scale MIMO: Far-field or near-field?" *IRE Trans. Commun.*, vol. 70, no. 4, pp. 2663–2677, Apr. 2022.
- [9] Z. Wu and L. Dai, "Multiple access for near-field communications: SDMA or LDMA?" *IEEE J. Sel. Areas Commun.*, early access.
- [10] S. Eslami, B. Gouda, and A. Tölli, "Near-field MIMO channel reconstruction via limited geometry feedback," in *ICASSP 2024 - 2024 IEEE International Conference on Acoustics, Speech and Signal Processing (ICASSP)*, 2024, pp. 9256–9260.
- [11] S. Eslami, B. Gouda, A. Tölli, and D. Kumar, "Geometry-aided joint estimation of short range MIMO channels with hybrid transceivers," in *2023 IEEE International Conference on Communications Workshops (ICC Workshops)*, 2023, pp. 1204–1209.
- [12] N. J. Myers, J. Kaleva, A. Tölli, and R. W. Heath, "Message passing-based link configuration in short range millimeter wave systems," *IEEE Transactions on Communications*, vol. 68, no. 6, pp. 3465–3479, 2020.
- [13] A. M. Elbir, K. Vijay Mishra, and S. Chatzinotas, "NBA-OMP: Near-field beam-split-aware orthogonal matching pursuit for wideband thz channel estimation," in *ICASSP 2023 - 2023 IEEE International Conference on Acoustics, Speech and Signal Processing (ICASSP)*, 2023, pp. 1–5.
- [14] H. V. Poor, *An Introduction to Signal Detection and Estimation (2nd Ed.)*. Berlin, Heidelberg: Springer-Verlag, 1994.
- [15] D. Gürünoğlu, E. Björnson, and G. Fodor, "Joint pilot-based localization and channel estimation in ris-aided communication systems," *IEEE Wireless Communications Letters*, vol. 13, no. 11, pp. 3119–3123, 2024.
- [16] N. Babu, A. Kosasih, C. Masouros, and E. Björnson, "Symbol-level precoding for near-field ISAC," *IEEE Commun. Lett.*, vol. 28, no. 9, pp. 2041–2045, 9 2024.
- [17] R. Schmidt, "Multiple emitter location and signal parameter estimation," *IEEE Transactions on Antennas and Propagation*, vol. 34, no. 3, pp. 276–280, 1986.
- [18] S. M. Kay, *Fundamentals of Statistical Signal Processing, Volume I: Estimation Theory*. Prentice Hall, 1993.